DOI: 10.1002/chem.200500941

Both Spacer Length and Parity Influence the Thermal and Light-Induced Properties of Iron(II) α,ω-Bis(tetrazole-1-yl)alkane Coordination Polymers

Alina Absmeier,[a, c] Matthias Bartel,[a, b] Chiara Carbonera,[c] Guy N. L. Jameson,[a] Peter Weinberger,[a] Andrea Caneschi,[b] Kurt Mereiter,[d] Jean-François Létard,[c] and Wolfgang Linert*[a]

Abstract: A new series of [μ-tris-{1,*n*-bis(tetrazol-1-yl)alkane-N4,N4′}iron(II)] bis(perchlorate) spin-crossover coordination polymers ($[Fe(n\text{ditz})_3](ClO_4)_2$; $n=4$–9) has been synthesised and characterised. The ditetrazole bridging ligands provide octahedral symmetry at the iron(II) centres while allowing the distance between iron(II) centres to be varied. These polymers have therefore been investigated to determine the effects of spacer length on their thermal and light-induced spin-transition behaviour. An increase in the number of carbon atoms in the spacer (*n*) raises the thermal spin-crossover temperature, while decreasing the stability of the light-induced metastable state generated through the light-induced excited spin state trapping (LIESST) effect by irradiating the sample at 530 nm. Remarkably, however, the parity of the spacer also has an effect, enabling the series of complexes to be divided into two sub-series depending on whether the bridging ligand possesses an even or an odd number of carbon atoms. An explanation at the molecular level using the single configurational coordinate (SCC) model is presented.

Keywords: iron · magnetic properties · nitrogen heterocycles · organic–inorganic hybrid composites · photo-magnetism · spin crossover

Introduction

Compounds that are able to switch their magnetic properties through changes in external conditions (e.g. temperature, pressure, light, etc.) have been studied for many years[1,2] because of their potential application in data-storage systems. In such systems, optical switching is particularly promising because of the high speed and ease of writing and reading information. This mode of switching thermally induced spin-crossover (SC) compounds was made possible following the discovery of light-induced excited spin state trapping (LIESST), which allows the spin state of an iron(II) centre to be changed from low spin (LS) to high spin (HS) and then restored through the reverse LIESST phenomenon.[3,4] The major drawback of this process is that although the lifetime of the photo-induced HS state is almost infinite below approximately 50 K, at higher temperatures the decay increases rapidly, thus making data storage impossible. It is therefore important to identify and understand the nature of the parameters affecting the stability of the photo-induced state,[5,6] and indeed many different complexes have been studied for the LIESST effect. Of those containing iron(II), however, the majority use terminal ligands[3,7–9] and are thus only able to form mononuclear complexes. Notable exceptions involve dimers[10,11] and a mixed-metal bridging system with a 2D layered structure.[12] Furthermore, a few systems have been investigated with a homologous series of ligands, which would allow a more systematic approach to the study of the various influences of the ligand.

Iron(II) spin-crossover compounds have been produced with many different N-coordinating heterocyclic ligands, such as triazoles,[13] tetrazoles[3,7–9,14] and imidazoles.[15] In

[a] A. Absmeier, M. Bartel, Dr. G. N. L. Jameson, Dr. P. Weinberger, Prof. Dr. W. Linert
Institute of Applied Synthetic Chemistry
Vienna University of Technology
Getreidemarkt 9/163-AC, 1060 Vienna (Austria)
Fax: (+43) 1-58801-16299
E-mail: wlinert@mail.zserv.tuwien.ac.at

[b] M. Bartel, Prof. Dr. A. Caneschi
LAMM, Dipartimento di Chimica & UdR INSTM
Università di Firenze
Via della Lastruccia 3, 50019 Sesto F.no (Italy)

[c] A. Absmeier, Dr. C. Carbonera, Prof. Dr. J.-F. Létard
Institut de Chimie de la Matière Condensée de Bordeaux
UPR CNRS No 9048, Université Bordeaux 1
Groupe des Sciences Moléculaires
87 Av. du Doc. A. Schweitzer, 33608 Pessac (France)

[d] Prof. Dr. K. Mereiter
Institute for Chemical Technologies and Analytics
Vienna University of Technology
Getreidemarkt 9/164-SC, 1060 Vienna (Austria)

particular, tetrazole-containing ligands have been successfully employed as part of a family[16] of terminal and bridging ligands to give mononuclear complexes[3,7–9] and within bridging ligands to form 1D chain structures[17,18] and 3D networks.[14] The latter, [μ-tris-{1,4-bis(tetrazol-1-yl)butane-N4,N4′}iron(II)] bis(hexafluorophosphate) ($[Fe(4ditz)_3](PF_6)_2$), proved to be particularly interesting. Each iron(II) centre is octahedrally coordinated by symmetry-equivalent tetrazole rings with the butylene spacer outstretched, thereby assuming a zigzag *trans* configuration spanning iron(II) centres (see Figure 1). The ditetrazole ligands link the iron(II) atoms into a 3D network, and three such 3D networks interpenetrate each other. This structure results in cooperativity between the iron(II) centres, as borne out by SQUID measurements. The compound has a two-step spin transition at 168 K (with a hysteresis of 5 K) and 173 K.[14] While the shorter ethylene-bridged ligand 1,2-bis(tetrazol-1-yl)ethane produces a 1D polymeric chain structure,[18] it was thought possible that longer alkyl spacers ($n>4$, where n is the number of carbon atoms in the spacer) might allow more interlocking networks and therefore exhibit interesting new effects.

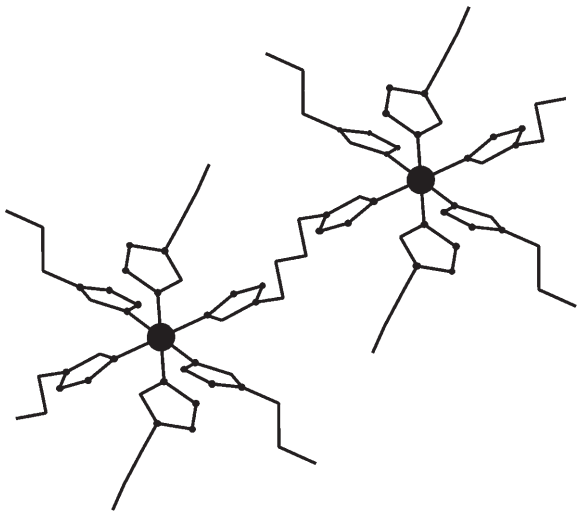

Figure 1. The basic structural units of $[Fe(4ditz)_3](PF_6)_2$ showing how the ligands span the iron(II) centres to produce a three-dimensional polymer.

We present here a detailed study of a series of α,ω-bis(tetrazole-1-yl)alkane iron(II) bis(perchlorate) coordination polymers in which the alkane is varied in the series from butane to nonane ($n=4$–9). All compounds have been characterised by UV/Vis-NIR and FTIR spectroscopy, reflectivity experiments, SQUID and LIESST. The effect of the spacer length and also the parity of the spacer on the thermal and light-induced properties in particular are discussed.

Experimental Section

Chemicals and standard physical characterisation: L-Ascorbic acid, 1,5-diaminopentane (>98%), 1,7-diaminoheptane (99%), 1,9-diaminononane (99%), glacial acetic acid (99%), iron(II) perchlorate hexahydrate, sodium azide, sodium hydroxide (97%) and triethyl orthoformate were obtained from Aldrich. All other chemicals were standard reagent grade and used as supplied.

Elemental analyses (C, H and N) were performed by the Mikroanalytisches Laboratorium, Faculty of Chemistry, Vienna University, Währingerstrasse 42, 1090 Vienna, Austria. ^{1}H and ^{13}C NMR spectra in [D$_6$]DMSO were measured with Bruker DPX 200 MHz or Bruker 250 FS FT-NMR spectrometers. ^{1}H NMR chemical shifts are reported in ppm calibrated to the respective solvent. Mid-range FTIR spectra of the compounds were recorded as KBr pellets in the range 4400–450 cm^{-1} with a Perkin–Elmer 16PC FTIR spectrometer. Pellets were obtained by pressing a powdered mixture of the samples in KBr in vacuo in a hydraulic press at a pressure of 10000 kg cm^{-2} for 5 min. Far-range FTIR spectra were recorded in the range 600–250 cm^{-1} on a Perkin–Elmer System 2000 Far-FTIR spectrometer. The complexes were diluted with polyethylene and pressed at a pressure of 10000 kg cm^{-2} transiently. Variable-temperature far-IR spectra in the temperature range 100–298 K were recorded with a Graseby–Specac thermostattable sample holder with polyethylene windows, attached to a Graseby–Specac automatic temperature controller.

Synthesis and crystallographic studies of the ligands: The general synthetic pathway and the synthesis of the even-numbered ligands 4ditz, 6ditz and 8ditz have been reported in the literature.[19,20] Modified procedures were used to produce three odd-numbered ligands 1,5-bis(tetrazol-1-yl)-pentane (5ditz), 1,7-bis(tetrazol-1-yl)heptane (7ditz) and 1,9-bis(tetrazol-1-yl)nonane (9ditz), as described below.

The respective diamine (80 mmol), sodium azide (160 mmol) and triethyl orthoformate (160 mmol) were stirred in a 500-mL, three-necked, round-bottomed flask. Acetic acid (250 mL, 99.5%) was then added and the mixture heated to 90–95 °C for four hours. After 4 and 16 h reaction time another aliquot of triethyl orthoformate (160 mmol) and sodium azide (160 mmol) was added and the mixture stirred for an additional 24 h at 95 °C. After cooling, the reaction mixture was poured into a beaker and a saturated sodium hydrogencarbonate solution was added with vigorous stirring to neutralise the acetic acid, followed by solid sodium hydrogencarbonate to precipitate the product. The suspension was cooled to 4 °C for 3 h and the precipitate was filtered off and recrystallised from ethanol. The colourless needle-shaped crystals were dried over P_2O_5. For all three compounds the mid-FTIR spectra show prominent absorptions at 3115 cm^{-1} (ν_{C1-H1} of the aromatic tetrazole ring); 2950/2940/2939 and 2870/2865/2849 cm^{-1} (ν_{C-H} of the aliphatic C–H in the pentylene/heptylene/nonylene spacer); and 1790/1792/1793, 1490/1491/1492, 1460/1464/1463 and 1175/1174 cm^{-1} (typical ν_{C-C} and ν_{C-N} of the tetrazole rings in 5ditz/7ditz/9ditz). The single crystals used for X-ray diffraction were obtained by solvent evaporation from an ethanol solution (5ditz), a pyridine solution (7ditz) or a DMF solution (9ditz).

5ditz: Yield: 10%; m.p. 125–127 °C; ^{1}H NMR (250 MHz, [D$_6$]DMSO): $\delta=9.39$ (s, 2H), 4.44 (t, $J=7.03$ Hz, 4H), 1.86 (quin, $J=7.19$ Hz, 4H), 1.18 ppm (quin, $J=7.62$ Hz, 2H); ^{13}C NMR (50 MHz, [D$_6$]DMSO): $\delta=$ 143.8 (d, 2C), 47.1 (t, 2C), 28.3 (t, 2C), 22.4 ppm (t, 2C); elemental analysis calcd (%) for $C_7H_{12}N_8$: C 40.38, H 5.81, N 53.81; found: C 40.65, H 5.72, N 53.52.

7ditz: Yield: 6.4%; m.p. 85–86 °C; ^{1}H NMR (200 MHz, [D$_6$]DMSO): $\delta=$ 9.38 (s, 2H), 4.43 (t, $J=7.05$ Hz, 4H), 1.81 (quin, $J=7.09$ Hz, 4H), 1.22 ppm (m, 6H); ^{13}C NMR (50 MHz, [D$_6$]DMSO): $\delta=143.7$ (d, 2C), 47.3 (t, 2C), 28.9 (t, 2C), 27.4 (t), 25.4 ppm (t, 2C); elemental analysis calcd (%) for $C_9H_{16}N_8$: C 45.75, H 6.83, N 47.42; found: C 45.97, H 6.90, N 47.32.

9ditz: Yield: 22.3%; m.p. 92–93 °C; ^{1}H NMR (200 MHz, [D$_6$]DMSO): $\delta=$ 9.39 (s, 2H), 4.43 (t, $J=7.14$ Hz, 4H), 1.81 (quin, $J=7.17$ Hz, 4H), 1.21 ppm (m,10H); ^{13}C NMR (50 MHz, [D$_6$]DMSO): $\delta=143.7$ (d, 2C), 47.4 (t, 2C), 29.0 (t, 2C), 28.4 (t), 28.0 (t, 2C), 25.5 ppm (t, 2C); elemental analysis calcd (%) for $C_{11}H_{20}N_8$: C 49.98, H 7.63, N 42.39; found: C 50.06, H 7.73, N 42.32.

Crystals of 5ditz, 7ditz and 9ditz were all elongated, lath-like and soft. Selected crystals were mounted on a Bruker SMART diffractometer (graphite-monochromated $Mo_{K\alpha}$ radiation from a sealed X-ray tube, $\lambda=$

0.71073 Å, platform three-circle goniometer, CCD area detector) and intensity data were collected at room temperature. After raw data extraction with the program SAINT, absorption and related effects were corrected with the program SADABS (multi-scan method) and data were processed with XPREP.[21] The structures were then solved by direct methods using SHELXS-97 followed by structure refinements on F^2 with SHELXL-97.[22] Non-hydrogen atoms were refined anisotropically. Hydrogen atoms were inserted in calculated positions and refined with the riding model. Crystallographic data are given in Table 1 and ORTEP plots are given in Figure 2 with the corresponding even ligands. CCDC-268788 (5ditz), CCDC-268789 (7ditz), and CCDC-268790 (9ditz) contain the supplementary crystallographic data for this paper. These data can be obtained free of charge from the Cambridge Crystallographic Data Centre via www.ccdc.cam.ac.uk/data_request/cif.

Table 1. Crystallographic data of 5ditz, 7ditz and 9ditz.

	5ditz	7ditz	9ditz
formula	$C_7H_{12}N_8$	$C_9H_{16}N_8$	$C_{11}H_{20}N_8$
molecular weight	208.25	236.30	264.35
crystal size [mm]	0.60×0.22×0.20	1.00×0.25×0.04	1.00×0.25×0.04
space group	*Fdd*2 (no. 43)	*Fdd*2 (no. 43)	*Fdd*2 (no. 43)
a [Å]	14.111(2)	13.738(2)	13.393(4)
b [Å]	32.041(4)	38.770(7)	45.260(13)
c [Å]	4.5613(6)	4.6300(8)	4.6724(14)
V [Å^3]	2062.3(5)	2466.0(7)	2832.4(15)
Z	8	8	8
ρ_{calcd} [g cm^{-3}]	1.341	1.273	1.240
T [K]	297(2)	297(2)	297(2)
μ [mm^{-1}] (Mo K_α)	0.095	0.088	0.084
F(000)	880	1008	1136
θ_{max} [°]	25	30	25
no. of reflections measured	4273	8879	6658
no. of unique reflections	912	1788	1240
no. of reflections $I>2\sigma(I)$	885	1365	984
no. of parameters	69	78	87
R_1 ($I>2\sigma(I)$)[a]	0.0444	0.0391	0.0547
R_1 (all data)	0.0462	0.0558	0.0726
wR_2 (all data)	0.1083	0.1069	0.1549
difference Fourier peaks min./max. [e Å^{-3}]	−0.11/0.12	−0.10/0.12	−0.13/0.22

[a] $R_1=\Sigma||F_o|-|F_c||/\Sigma|F_o|$, $wR_2=[\Sigma(w(F_o^2-F_c^2)^2)/\Sigma(w(F_o^2)^2)]^{1/2}$.

Synthesis of the complexes: A similar procedure was used for the synthesis of all members of the series $[Fe(nditz)_3](ClO_4)_2$ (n = 4—9). The respective ligand (1 mmol) was dissolved in hot ethanol. While the solution cooled down to 40 °C, iron(II) perchlorate hexahydrate (0.33 mmol) and a small amount of ascorbic acid (to keep the iron as iron(II)) were diluted in ethanol (5 mL). This solution was slowly added to the dissolved ligand and the resulting mixture stirred for four hours. The precipitate was filtered off and the obtained powder dried over P_2O_5. Unfortunately, it has so far proved impossible to grow single crystals by any of the standard methods, including H-tube slow diffusion or slow cooling.

Elemental analyses and mid-FTIR data

$[Fe(4ditz)_3](ClO_4)_2$: Yield: 80%. Elemental analysis calcd (%) for $C_{18}H_{30}Cl_2FeN_{24}O_8$: C 25.82, H 3.61, N 40.15; found: C 26.59, H 3.58, N 39.36. Mid-FTIR: $\tilde{\nu}=3137$ (ν_{C1-H1} of the aromatic tetrazole ring); 2956 and 2875 (ν_{C-H} of the aliphatic C–H in the butylene spacer); 1784, 1651, 1470, 1445 and 1183 cm^{-1} (typical ν_{C-C} and ν_{C-N} of the tetrazole rings).

$[Fe(5ditz)_3](ClO_4)_2$: Yield: 82%. Elemental analysis calcd (%) for $C_{21}H_{36}Cl_2FeN_{24}O_8$: C 28.68, H 4.13, N 38.23; found: C 29.65, H 4.03, N 37.53. Mid-FTIR: $\tilde{\nu}=3135$ (ν_{C1-H1} of the aromatic tetrazole ring); 2947 and 2866 (ν_{C-H} of the aliphatic C–H in the pentylene spacer); 1787, 1649, 1459, 1445 and 1181 cm^{-1} (typical ν_{C-C} and ν_{C-N} of the tetrazole rings).

$[Fe(6ditz)_3](ClO_4)_2$: Yield: 76%. Elemental analysis calcd (%) for $C_{24}H_{42}Cl_2FeN_{24}O_8$: C 31.28, H 4.59, N 36.48; found: C 31.24, H 4.45, N 35.68. Mid-FTIR: $\tilde{\nu}=3137$ (ν_{C1-H1} of the aromatic tetrazole ring); 2935 and 2860 (ν_{C-H} of the aliphatic C–H in the hexylene spacer); 1781, 1636, 1452, 1438 and 1178 cm^{-1} (typical ν_{C-C} and ν_{C-N} of the tetrazole rings).

$[Fe(7ditz)_3](ClO_4)_2$: Yield: 43%. Elemental analysis calcd (%) for $C_{27}H_{48}Cl_2FeN_{24}O_8$: C 33.66, H 5.02, N 34.69; found: C 33.78, H 4.84, N 34.53. Mid-FTIR: $\tilde{\nu}=3137$ (ν_{C1-H1} of

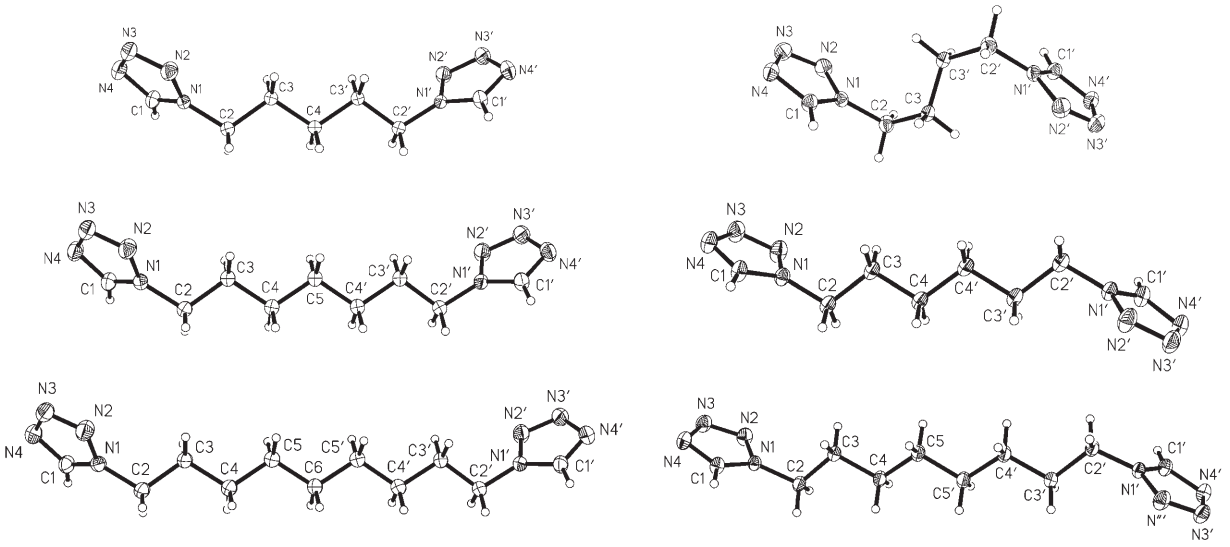

Figure 2. Structural views of 5ditz, 7ditz and 9ditz (20% probability ellipsoids). All molecules have C_2 symmetry with the twofold axis passing through C4, C5 and C6, respectively. 4ditz, 6ditz and 8ditz are shown to the right for comparison.[16]

the aromatic tetrazole ring); 2940 and 2864 (ν_{C-H} of the aliphatic C–H in the heptylene spacer); 1790, 1635, 1463, 1443 and 1180 cm^{-1} (typical ν_{C-C} and ν_{C-N} of the tetrazole rings).

$[Fe(8ditz)_3](ClO_4)_2$: Yield: 96%. Elemental analysis calcd (%) for $C_{30}H_{54}Cl_2FeN_{24}O_8$: C 35.83, H 5.41, N 33.43; found: C 36.64, H 5.16, N 32.88. Mid-FTIR: $\tilde{\nu}=3138$ (ν_{C1-H1} of the aromatic tetrazole ring); 2934 and 2859 (ν_{C-H} of the aliphatic C–H in the octylene spacer); 1792, 1645, 1457, 1440 and 1181 cm^{-1} (typical ν_{C-C} and ν_{C-N} of the tetrazole rings)

$[Fe(9ditz)_3](ClO_4)_2$: Yield: 86%. Elemental analysis calcd (%) for $C_{33}H_{60}Cl_2FeN_{24}O_8$: C 37.83, H 5.77, N 32.08; found: C 38.30, H 5.54, N 30.84. Mid-FTIR: $\tilde{\nu}=3138$ (ν_{C1-H1} of the aromatic tetrazole ring); 2929 and 2856 (ν_{C-H} of the aliphatic C–H in the nonylene spacer); 1798, 1650, 1462, 1444 and 1180 cm^{-1} (typical ν_{C-C} and ν_{C-N} of the tetrazole rings).

UV/Vis–NIR reflectivity: UV/Vis–NIR spectra were recorded with a Perkin–Elmer Lambda 900 UV/Vis–NIR spectrometer between 1500 and 300 nm using the method of diffuse reflection. A spectrum of $BaSO_4$ was subtracted as background. Variable-temperature measurements were made using a custom-made thermostattable sample holder with quartz glass windows within a spectralon integration sphere. The temperature was controlled with a Harrick controller. Aluminium foil was used to improve the thermal contact between the sample holder and the sample. The spectra were measured between 105 and 260 K in intervals of 5 to 10 K.

The reflectivity of the samples was further investigated with a custom-built reflectivity set-up equipped with a CVI spectrometer, which allows the collection of both the reflectivity spectra within the range of 450–950 nm at a given temperature and to follow the temperature dependence of the signal at a selected wavelength (±2.5 nm) at 5–290 K. The analysis was performed on a thin layer of the powdered sample without any dispersion in a matrix.[23]

Magnetic susceptibility and magneto-optical measurements: Magnetic measurements were recorded on two SQUID (Superconducting Quantum Interference Device) magnetometers as described hereafter: 1) SQUID Cryogenix S600 magnetometer with an applied field of 1 T; 2) MPMS-55 Quantum Design SQUID magnetometer with an operating field of 2 T within the temperature range of 2–300 K and with a speed of 10 K min^{-1} in the settle mode at atmospheric pressure. All measurements were performed on polycrystalline powder samples weighing about 12 mg. The data were corrected for the magnetisation of the sample holder and for diamagnetic contributions, estimated from Pascal's constants.

The photo-magnetic measurements were performed with a Spectra Physics Series 2025 Kr^+ laser ($\lambda=532$ nm) coupled by an optical fibre to the cavity of the SQUID magnetometer (MPMS-55 Quantum Design SQUID) operating with an external magnetic field of 2 T within the 2–300 K temperature range and a speed of 10 K min^{-1} in the settle mode at atmospheric pressure. The power at the sample was adjusted to 5 mW cm^{-2}. Bulk attenuation of light intensity was limited as much as possible by the preparation of a thin layer of compound. It is noteworthy that there was no change in the data due to sample heating upon laser irradiation. The weight of these thin layer samples (approximately 0.2 mg) was obtained by comparison of the measured thermal spin-crossover curve with another curve of a more accurately weighed sample of the same compound.

Results and Discussion

The coordination polymers described herein form a series that differ only in the length of the alkane spacer connecting the tetrazole moieties. Unfortunately, it was not possible, despite considerable effort, to produce single crystals suitable for X-ray diffraction studies. However, some general comments about the structure of these polymers can be made. Firstly, the structures can be compared with that of $[Fe(4ditz)_3](PF_6)_2$, which was published previously[19] and is described above (see also Figure 1). Preliminary powder X-ray diffraction investigations of the ClO_4^- and PF_6^- salts of $[Fe(4ditz)_3]$ show that they have a similar structure, with ClO_4^- having reduced symmetry due to compression along one or more axes. As the group is traversed, the anion and the method of production are kept constant, with only the alkane spacer changing. The crystal packing of all the free ligands is very similar, thereby suggesting a similar behaviour. Furthermore, the UV/Vis–IR data presented below show that the iron is octahedrally coordinated. Thus, although the presence or number of interpenetrating networks seen in $[Fe(4ditz)_3](PF_6)_2$ is unknown, it can be assumed that a 3D network of octahedrally coordinated iron centres, as shown in Figure 1, is present in all samples. Naturally, as the alkane spacer increases in length, the increase in degrees of freedom reduces the crystallinity of the samples (i.e. making them more amorphous). However, because the iron centres themselves are well defined, a non-crystalline structure in no way precludes important information being gained from measurement of the magnetic properties.

Magnetic properties: To study how the number of carbon atoms in the spacer of the ligand influences the spin transition, susceptibility curves were recorded between 10 and 300 K for all the complexes of the series. Figure 3 shows the obtained $\chi_M T$ versus T curves, where χ_M is the molar magnetic susceptibility and T is the temperature.

All the investigated products undergo a thermal spin-transition at around 150 K, from a $\chi_M T$ product close to 3.0 cm^{-3} K mol^{-1} at room temperature, in agreement with the expected HS state, and a diamagnetic value at low temperature reflecting the LS state. In some of the curves a residual magnetisation is observed at low temperatures, yielding a $\chi_M T$ value of up to 1 cm^{-3} K mol^{-1}, which might be caused by traces of iron(III) or thermally SC-inactive HS iron(II).

The temperature of the thermal spin-state transition, $T_{1/2}$, estimated from the maximum in the derivative of the $\chi_M T$ versus T plot is given in Table 2, and Figure 4a shows the change of $T_{1/2}$ with the length of the alkane spacer (n). Interestingly, an increase in the length of the spacer raises the $T_{1/2}$ value, but it can also be seen that the influence of the parity of the spacer is not negligible. Indeed, it seems that the complexes can be divided into two series depending on the parity of the spacer: the first, which contains bridging ligand with odd-numbered carbon atoms in the spacer, shows a $\chi_M T$ product at room temperature that is always equal to 3.0 cm^{-3} K mol^{-1}; the second series, with even-numbered spacers, exhibits a $\chi_M T$ at room temperature of approximately 3.75 cm^{-3} K mol^{-1}. A similar classification can also be made if we compare the shape of the thermal spin-transitions in Figure 3. Complexes with an odd-numbered spacer ($[Fe(5ditz)_3](ClO_4)_2$], $[Fe(7ditz)_3](ClO_4)_2$] and $[Fe(9ditz)_3](ClO_4)_2$]) display a more gradual transition than complexes with an even-numbered ligand ($[Fe(4ditz)_3](ClO_4)_2$, $[Fe(6ditz)_3](ClO_4)_2$ and $[Fe(8ditz)_3](ClO_4)_2$).

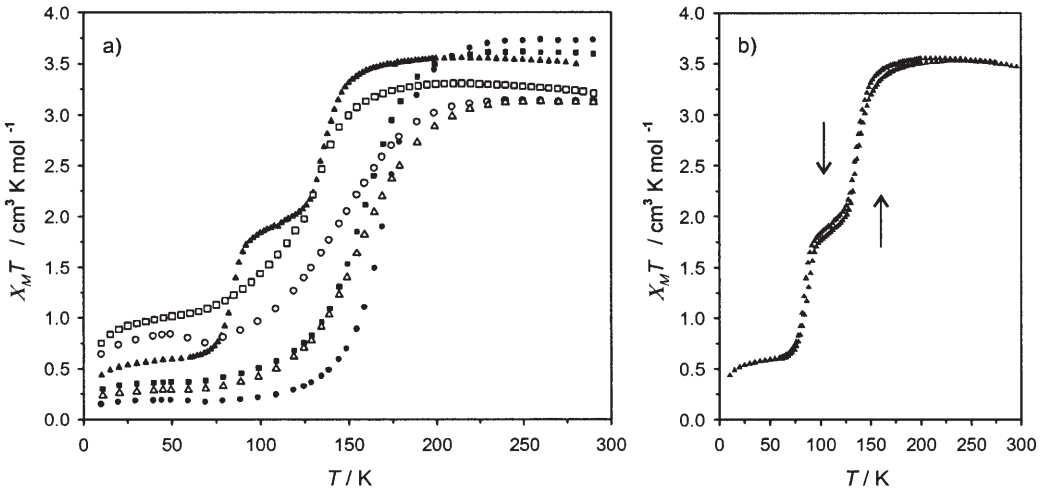

Figure 3. a) Temperature dependency of the $\chi_M T$ product for the investigated complexes $[Fe(4ditz)_3](ClO_4)_2$ (▲), $[Fe(5ditz)_3](ClO_4)_2$ (□), $[Fe(6ditz)_3](ClO_4)_2$ (■), $[Fe(7ditz)_3](ClO_4)_2$ (○), $[Fe(8ditz)_3](ClO_4)_2$ (●) and $[Fe(9ditz)_3](ClO_4)_2$ (△); b) cooling and heating modes for $[Fe(4ditz)_3](ClO_4)_2$.

Table 2. Spin-transition, reflectivity and LIESST parameters of the discussed complexes.

$[Fe(n\text{ditz})_3](ClO_4)_2$	$T_{1/2}$ [K]	T(LIESST) [K]	% Irr-surface[b]	% Irr-bulk[c]
$[Fe(4ditz)_3](ClO_4)_2$	84/ 134[a]	58/39	52	60
$[Fe(5ditz)_3](ClO_4)_2$	125	52	64	72
$[Fe(6ditz)_3](ClO_4)_2$	155	–	42	43
$[Fe(7ditz)_3](ClO_4)_2$	144	51	42	57
$[Fe(8ditz)_3](ClO_4)_2$	169	–	14	13
$[Fe(9ditz)_3](ClO_4)_2$	155	37	26	47

[a] Estimated at the maximum of the derivative of each of the two thermal spin-transitions. [b] Percentage of sample photo-bleached. [c] Percentage conversion to the metastable high-spin state by irradiation at 10 K.

However, within this classification the case of $[Fe(4ditz)_3](ClO_4)_2$ is somewhat exceptional in that it is the only one that displays a two-step thermal spin-transition with a plateau between 93 and 124 K (Figure 3a). This behaviour can be compared with the same complex synthesised in methanol solution and published previously by van Koningsbruggen et al.[19] The magnetic susceptibility curves of the two $[Fe(4ditz)_3](ClO_4)_2$ compounds (one synthesised in methanol and the other synthesised in ethanol) show clear differences in both the shape of the spin-transition curves and in their spin-transition behaviour. Indeed, the shape of the magnetic susceptibility curve of the compound made previously in methanol shows an incomplete one-step spin transition. This suggests a significant influence of the solvent and could be due to either inclusion of solvent, as observed previously in the $[Fe(2\text{-pic})_3]Cl_2$·solvent family of complexes,[24] or the production of different polymorphs according to the solvent. The effect of solvent on the present coordination polymers is currently being investigated further.

Optical and far-FTIR properties: As expected, all members of the series show a thermochromic effect associated with

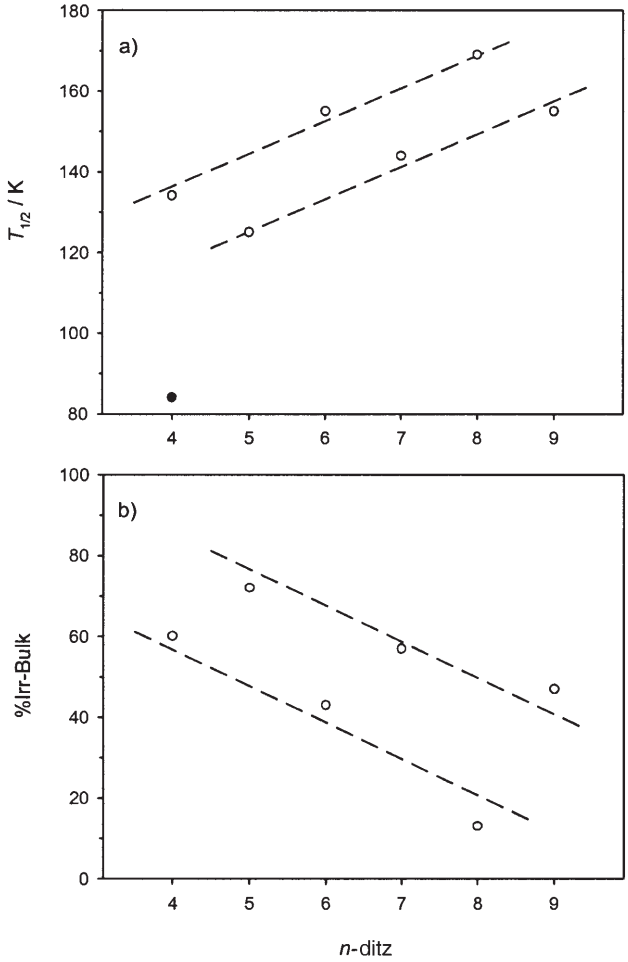

Figure 4. $T_{1/2}$ (a) and %Irr-Bulk (b) as a function of the number of carbons (n) in the spacer of the ditetrazole ligands. (●) indicates $T_{1/2}$ of the lower temperature spin-transition of $[Fe(4ditz)_3](ClO_4)_2$. The parallel dashed lines are drawn to clearly show the separation of the data points into two sub-series (even and odd) but have no further significance.

the spin transition, from white in the HS state to violet in the LS state. A typical temperature-dependent UV/VIS–NIR spectrum of these complexes is given in Figure 5. The spectrum shown is that of $[Fe(9ditz)_3](ClO_4)_2$ within the

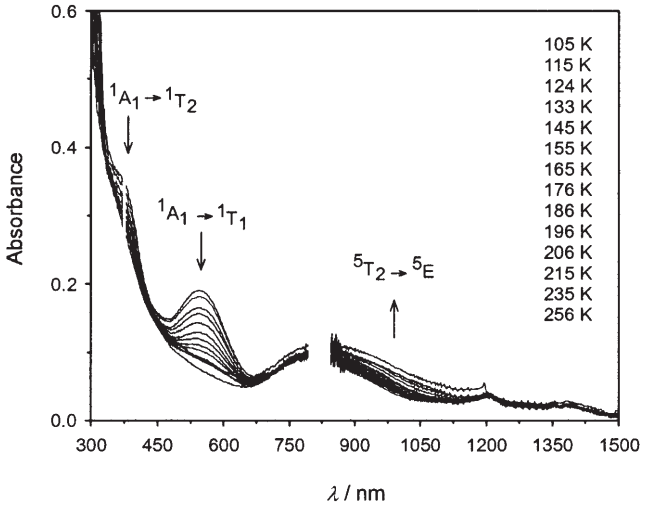

Figure 5. Temperature-dependent UV/VIS–NIR spectra of $[Fe(9ditz)_3](ClO_4)_2$ between 1500 and 300 nm. The gaps in the data occur because we have removed the large noise caused by changing grating and detector.

range 300–1500 nm and at temperatures between 105 and 256 K. The absorption spectrum is composed of one charge-transfer (CT) band at low wavelength and three recognisable peaks, two of which decrease and one that increases with increasing temperature. The peaks at 550 and 370 nm are d–d transitions of the LS state of the complex, the peak at 300 nm is a charge-transfer band of the ligand and the band at 1000 nm is the d–d transition of the HS state. According to the Tanabe–Sugano diagram for d^6 systems, the two LS transitions can be assigned to the spin-allowed transitions $^1A_1 \rightarrow {}^1T_2$ and $^1A_1 \rightarrow {}^1T_1$ and the HS band corresponds to the $^5T_2 \rightarrow {}^5E$ transition.

In parallel to this we used a custom-built reflectivity instrument to record the change occurring at 830 ± 2.5 nm and at 550 ± 2.5 nm, which are the wavelengths of the $^5T_2 \rightarrow {}^5E$ and the $^1A_1 \rightarrow {}^1T_1$ transitions, respectively, as a function of temperature (290–10 K) and also light irradiation. The results of a typical experiment are shown in Figure 6 for $[Fe(5ditz)_3](ClO_4)_2$.

In agreement with the previous UV-VIS–NIR study, within the range of 450–950 nm only the HS band is visible at room temperature for all compounds, whilst at 80 K only the LS transition is observable. Below 80 K, however, the reflectivity experiment demonstrates the existence of a photo-induced phenomenon at the surface. In fact, at low temperatures the sample was seen to bleach (see, for example, Figure 6 and insert), which indicates the occurrence of a LS/HS photo-conversion through the LIESST effect. We have calculated the amount of photo-bleached fraction (%Irr-Surface; reported in Table 2) for each compound relative to the value found at room temperature. Interestingly, the level of photo-excitation roughly decreases with the length of the spacer.

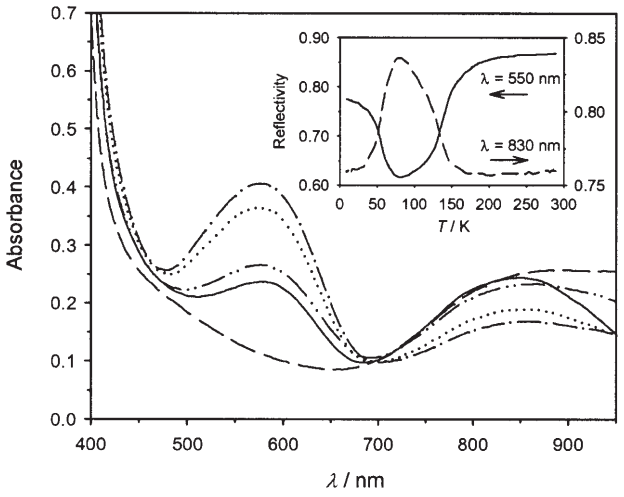

Figure 6. Reflectivity measurements of $[Fe(5ditz)_3](ClO_4)_2$ as a function of temperature. The absorbance spectra at 280 (– – –), 140 (–···–), 80 (–•–•–), 60 (•••••) and 10 K (——) are shown in the main figure. The insert reports the reflectivity followed at 550 ± 2.5 nm and 830 ± 2.5 nm.

It cannot be excluded that other parameters, such as the morphology of the powder particles, should be taken into account in order to discuss the problem of the light penetration, but it is clear that the level of photo-excitation follows the increase of the $T_{1/2}$ value: the higher the $T_{1/2}$, the lower is the level of the light-induced LS/HS conversion. This result can, in fact, be discussed in terms of the inverse energy-gap law introduced by Hauser.[25] In the so-called single configurational coordinate (SCC) model, the potential wells of the LS and HS states are plotted along a single reaction coordinate Q, which describes the totally symmetric breathing mode and is related to the metal–ligand bond difference by $\Delta Q = \sqrt{6}\Delta r$ (see Figure 7). The potential wells and their shape can, therefore, be moved horizontally relative to each other by changing the relative bond strengths of HS and LS, or the wells can be moved vertically relative to each other.

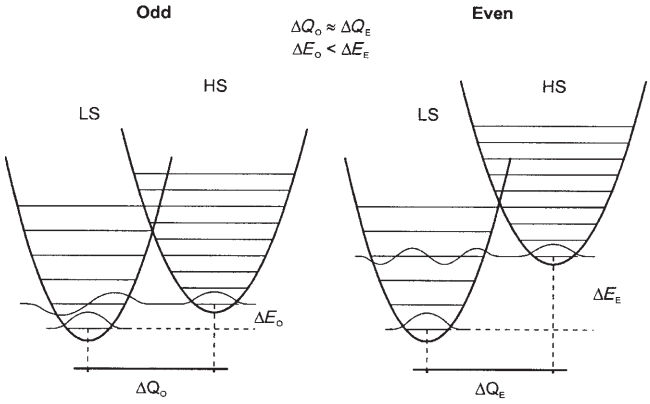

Figure 7. Potential wells for an odd and even ditetrazole coordination polymer demonstrating the effect of the parity of the bridging ligand. Only ΔE appears to be affected and not ΔQ.

The difference in the zero-point energies of LS and HS, ΔE, is therefore related to $T_{1/2}$. We therefore recorded the far-FTIR spectra of all the members of the $[Fe(n\text{ditz})_3](ClO_4)_2$ series; interestingly, almost no difference was observed (see Table 3). Strikingly, the LS state shows a band that only varies between 421 and 424 cm^{-1} and the HS state shows bands that vary by a maximum of 10 cm^{-1} and certainly do not follow any obvious trend. From that we can conclude that the shape of the potential wells of the LS and the HS states, as well as the horizontal distance between them (ΔQ), can be considered almost the same for all complexes. In other words, along the $[Fe(n\text{ditz})_3](ClO_4)_2$ series the change in $T_{1/2}$ implies a vertical displacement of the two potential wells and hence a variation in ΔE with the parity, as shown in Figure 7.

Table 3. Temperature-dependent far-IR bands that can be associated with HS and LS species of $[Fe(n\text{ditz})_3](ClO_4)_2$.

n	HS	LS
5	469(w), 388(w), 367(m)	421(s), 380(w), 358(sh), 287(s)
6	476(m), 378(s), 357(sh), 282(sh)	422(m), 393(s), 364(m)
8	437(sh), 373(m), 338(m), 310(sh)	424(s), 395(w), 379(w), 354(s)
9	366(sh), 331(sh)	422(s), 354(m)

A further consequence of the variation of ΔE can be explained as it has previously been shown that there is a direct relationship between the rate constant of tunnelling, k_o, and $T_{1/2}$.[26] Based on this finding we can see that if the stability of the photo-induced HS state decreases with the increase of $T_{1/2}$ (and of ΔE), for a constant intensity of light irradiation, the photo-excitation becomes more and more difficult, as observed experimentally (%Irr-Surface; reported in Table 2).

Photo-magnetic properties: The photo-magnetic properties of the different compounds were investigated by following the effect of irradiation with light under the influence of an applied magnetic field. At first, the sample was cooled slowly down to 10 K in order to stabilise the low-spin state; it was then irradiated and the change in magnetism was followed. When the saturation point was reached the light was switched off, the temperature was increased at a rate of 0.3 K min^{-1} and the magnetisation measured every 1 K. This procedure allows the quantification of T(LIESST), which is determined by the minimum of the $\partial\chi_M T/\partial T$ versus T curve recorded during relaxation.[5] Figure 8 shows the photo-magnetic behaviour together with the magnetic susceptibility for each compound for the sake of completeness.

Table 2 collects, for each compound, the highest percentage of photo-conversion obtained by irradiation at 10 K relative to the magnetic value recorded at room temperature for a pure HS state (%Irr-Bulk). As expected from the surface analysis, we can see here that with bulk detection the level of photo-excitation is not uniform for all the compounds, even when special attention was paid to tune the intensity and/or the wavelength. This confirms once more that the level of photo-excitation decreases with an increase of $T_{1/2}$ and therefore clearly shows the influence of both the length and parity of the bridging ligand (see Figure 4).

If we now compare the shape of the T(LIESST) curve recorded by increasing the temperature, the complexes continue to behave differently from one other. For those with a short spacer, the $\chi_M T$ product increases in the 10–30 K range, while for long spacers the magnetic signal strongly decreases. This behaviour provides new evidence that the stability of the photo-induced HS state in the tunnelling region varies along the $[Fe(n\text{ditz})_3](ClO_4)_2$ series. In fact, only for complexes possessing a sufficiently long-lived lifetime does the photo-induced HS fraction remain almost independent of any change of the temperature and of the effect of time during the measurement of the T(LIESST) curve. Consequently, the $\chi_M T$ curve displays an increase in the magnetic response with the temperature due to the effect of the zero-field splitting (ZFS) of the iron(II) HS state in a non-perfectly octahedral geometry.[27] Indeed, the series of odd-numbered ligands show a ZFS effect that progressively vanishes in the order $[Fe(5ditz)_3](ClO_4)_2 > [Fe(7ditz)_3](ClO_4)_2 > [Fe(9ditz)_3](ClO_4)_2$, thereby reflecting a decrease of the lifetime of the photo-induced HS state in the tunnelling region.

An additional way to see the stability of the photo-induced HS state is to compare the magnitude of the T(LIESST) temperatures.[5,6] Table 2 collects T(LIESST) temperatures of the $[Fe(n\text{ditz})_3](ClO_4)_2$ family, with the exception of the complexes $[Fe(6ditz)_3](ClO_4)_2$ and $[Fe(8ditz)_3](ClO_4)_2$, where the minimum on the $\partial\chi_M T/\partial T$ versus T curve cannot be properly determined due to the very low efficiency of the photo-excitation (Figure 8). Nevertheless, it is interesting to see that the lowest T(LIESST) is found for $[Fe(9ditz)_3](ClO_4)_2$, which presents the highest $T_{1/2}$ value, as expected from the previous discussion of the stability of the photo-induced HS state.

Finally, it is important to note that the peculiarity of $[Fe(4ditz)_3](ClO_4)_2$, which is characterised by a two-step thermal spin-transition, shows similar features in the T(LIESST) experiments. Analysis of the $\partial\chi_M T/\partial T$ versus T curve clearly shows the existence of two minima, at 39 K and 58 K, thus proving that both magnetically non-equivalent iron(II) metal centres can be photo-excited. It is also reasonable to propose that the T(LIESST) temperature found at 58 K corresponds to photo-excitation of the iron(II) metal centres involved in the LS/HS thermal spin-transition occurring at 84 K, and the T(LIESST) temperature at 39 K is linked to an SC phenomenon occurring at 134 K. The presence of two minima on the T(LIESST) curve is not unexpected as a similar result has been found for a mononuclear iron(II) SC material that also displays a two-step thermal spin-transition.[28]

Conclusion

We have presented the first systematic study of a homologous series of iron(II) spin-crossover coordination polymers

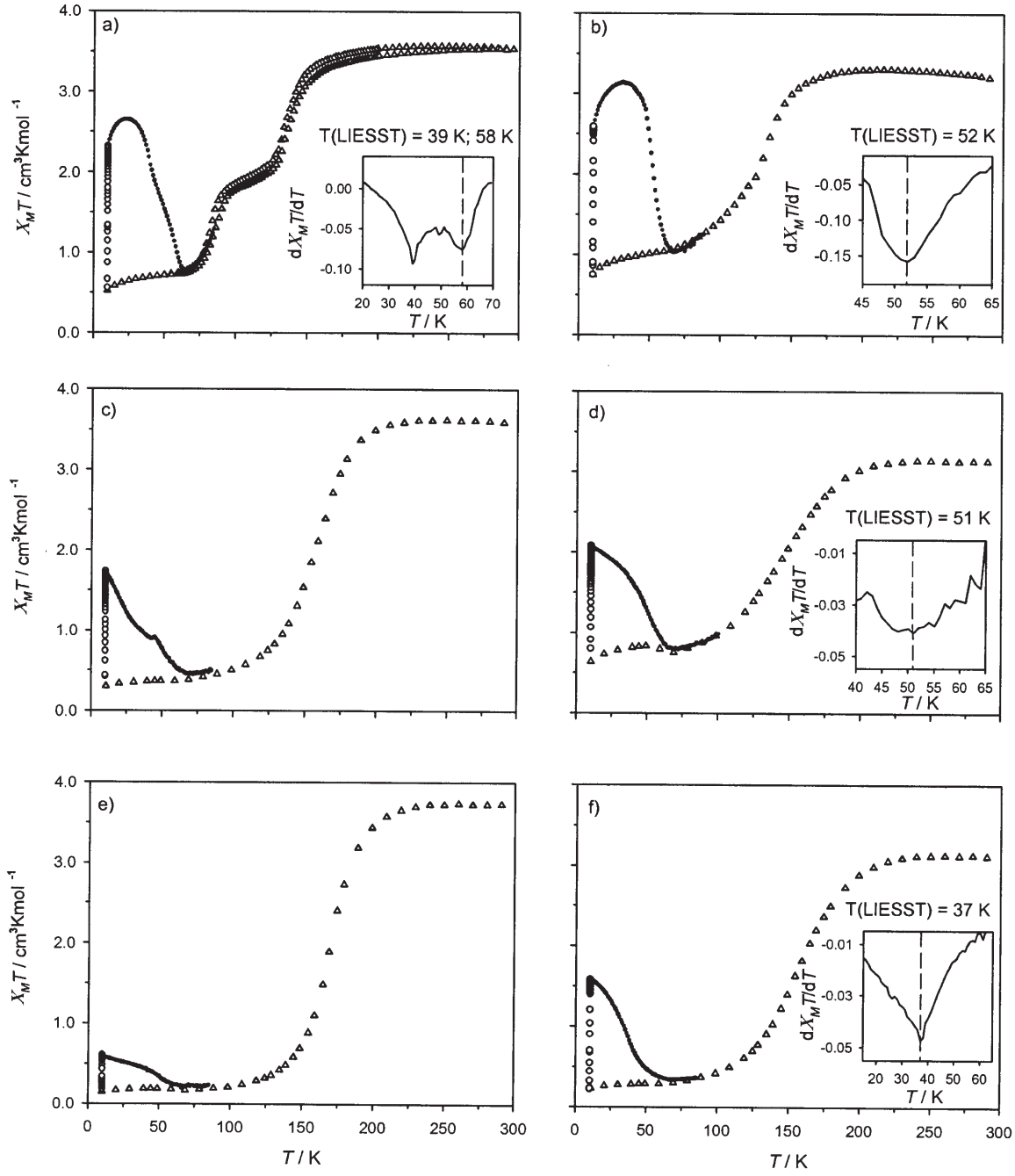

Figure 8. Temperature dependence of $\chi_M T$ for a) $[Fe(4ditz)_3](ClO_4)_2$, b) $[Fe(5ditz)_3](ClO_4)_2$, c) $[Fe(6ditz)_3](ClO_4)_2$, d) $[Fe(7ditz)_3](ClO_4)_2$, e) $[Fe(8ditz)_3](ClO_4)_2$ and f) $[Fe(9ditz)_3](ClO_4)_2$. (△) Data recorded without irradiation; (○) data recorded with irradiation at 10 K; (●) T(LIESST) measurement, data recorded in the warming mode with the laser turned off after irradiation for one hour. (Note that the small bump at 49 K observable in (c) is due to a small amount of dioxygen).

containing ClO_4^- as counteranion and have demonstrated that for the $[Fe(n\text{ditz})_3](ClO_4)_2$ ($n=4$–9) series both the length and parity of the spacer have a large and systematic influence on the magnetic and photo-magnetic properties. With the exception of $[Fe(4ditz)_3](ClO_4)_2$, we have shown a two-step transition that is similar to the previously published compound obtained with PF_6^- as anion.[14] This behaviour contrasts with $[Fe(2ditz)_3(BF_4)_2]$, which is known to display an incomplete gradual thermal spin-transition at about 140 K.[18] A butylene group between the tetrazoles seems to provide the ideal distance between iron(II) centres that allows an interpenetrated network structure to be formed. In the case of longer spacers, the thermal spin-transition is also gradual, although whether this is due to structural changes is still unclear. Unfortunately, we have not been able to obtain single crystals of these coordination polymers.

From our magnetic studies, we have provided evidence to show that the thermal spin-transition temperature increases

with the number of carbon atoms (n) in the spacer and we have reported a fascinating effect of the parity. The complexes with an even "n" display a more abrupt spin transition than odd-numbered ones. The $T_{1/2}$ values have also been found to be higher for the complexes having even-numbered $n$ditz ligands than for the odd-numbered ligands.

From our photo-magnetic investigations, we have also highlighted that the LIESST properties of the $[Fe(n\text{ditz})_3](ClO_4)_2$ family are strongly affected by the parity of the bridging ligands. Based on the SCC model in combination with far-FTIR spectroscopic data, we have proposed that the energy difference between the LS and the HS states is higher for the even series. Moreover, we have experimentally observed that the level of photo-excitation, as well as the T(LIESST) temperature, perfectly follow the tendency defined by $T_{1/2}$.

Acknowledgements

Financial support from the Austrian Science Foundation FWF (project 15874-N03) and the Italian MIUR, FIRB and PRIN projects is gratefully acknowledged. Furthermore, we thank the EU COST D14 action project 0011/01 for granting A. Absmeier a "Short Term Scientific Mission" in Bordeaux. Additionally, M. Bartel carried out research in Florence within the Marie Curie Training site LAMM (MOLMAG-MEST-CT-2004-504204).

[1] *Molecular Magnets: Recent Highlights* (Eds.: W. Linert, M. Verdaguer), Springer, Wien, **2003**.
[2] *Spin Crossover in Transition Metal Compounds Vols. I–III*, in *Topics in Current Chemistry* (Eds.: P. Gütlich and H. A. Goodwin), Springer, Berlin, **2004**.
[3] S. Decurtins, P. Gütlich, K. M. Hasselbach, H. Spiering, A. Hauser, *Inorg. Chem.* **1985**, *24*, 2174–2178.
[4] A. Hauser, P. Gütlich, H. Spiering, *Inorg. Chem.* **1986**, *25*, 4245–4248.
[5] J.-F. Létard, L. Capes, G. Chastanet, N. Moliner, S. Létard, J.-A. Real, O. Kahn, *Chem. Phys. Lett.* **1999**, *313*, 115–120.
[6] J.-F. Létard, P. Guionneau, O. Nguyen, J. S. Costa, S. Marcén, G. Chastanet, M. Marchivie, L. Goux-Capes, *Chem. Eur. J.* **2005**, *11*, 4582–4589.
[7] P. Poganiuch, S. Decurtins, P. Gütlich, *J. Am. Chem. Soc.* **1990**, *112*, 3270–3278.
[8] Th. Buchen, P. Gütlich, *Chem. Phys. Lett.* **1994**, *220*, 262–266.
[9] A. F. Stassen, O. Roubeau, I. F. Gramage, J. Linares, F. Varret, I. Mutikainen, U. Turpeinen, J. G. Haasnoot, J. Reedijk, *Polyhedron* **2001**, *20*, 1699–1707.
[10] G. Chastanet, A. B. Gaspar, J. A. Real, J. F. Létard, *Chem. Commun.* **2001**, 819–820.
[11] A. B. Gaspar, V. Ksenofontov, H. Spiering, S. Reiman, J. A. Real, P. Gütlich, *Hyperfine Interact.* **2002**, *144/145*, 297–306.
[12] V. Niel, A. Galet, A. B. Gaspar, M. C. Munoz, J. A. Real, *Chem. Commun.* **2003**, 1248–1249.
[13] J. G. Haasnoot, *Coord. Chem. Rev.* **2000**, *200–202*, 131–185.
[14] C. M. Grunert, J. Schweifer, P. Weinberger, W. Linert, K. Mereiter, G. Hilscher, M. Muller, G. Wiesinger, P. J. van Koningsbruggen, *Inorg. Chem.* **2004**, *43*, 155–165.
[15] Y. Sunatsuki, H. Ohata, M. Kojima, Y. Ikuta, Y. Goto, N. Matsumoto, S. Iijima, H. Akashi, S. Kaizaki, F. Dahan, J.-P Tuchagues, *Inorg. Chem.* **2004**, *43*, 4154–4171.
[16] C. M. Grunert, P. Weinberger, J. Schweifer, C. Hampel, A. F. Stassen, K. Mereiter, W. Linert, *J. Mol. Struct.* **2005**, *733*, 41–52.
[17] P. J. van Koningsbruggen, Y. Garcia, O. Kahn, L. Fournes, H. Kooijman, A. L. Spek, J. G. Haasnoot, J. Moscovici, K. Provost, A. Michalowicz, F. Renz, P. Gütlich, *Inorg. Chem.* **2000**, *39*, 1891–1900.
[18] J. Schweifer, P. Weinberger, K. Mereiter, M. Boca, C. Reichl, G. Wiesinger, G. Hilscher, P. J. van Koningsbruggen, H. Kooijman, M. Grunert, W. Linert, *Inorg. Chim. Acta* **2002**, *339*, 297–306.
[19] P. J. van Koningsbruggen, Y. Garcia, H. Kooijman, A. L. Spek, J. G. Haasnoot, O. Kahn, J. Linares, E. Codjovi, F. Varret, *J. Chem. Soc. Dalton Trans.* **2001**, 466–471.
[20] P. L. Franke, J. G. Hasnoot, A. P. Zuur, *Inorg. Chim. Acta* **1982**, *59*, 5–9.
[21] Bruker (2001). Programs SMART, version 5.054; SAINT, version 6.2.9; SADABS version 2.03; XPREP, version 5.1; SHELXTL, version 5.1. Bruker AXS Inc., Madison, Wisconsin, USA.
[22] G. M. Sheldrick, Programs SHELXS97 and SHELXL97, University of Göttingen, Germany, **1997**.
[23] C. Carbonera, A. Dei, C. Sangregorio, J.-F. Létard, *Chem. Phys. Lett.* **2004**, *396*, 198–201.
[24] M. Hostettler, K. W. Törnroos, D. Chernyshov, B. Vangdal, H.-B. Bürgi, *Angew. Chem.* **2004**, *116*, 4689–4695; *Angew. Chem. Int. Ed.* **2004**, *43*, 4589–4594.
[25] A. Hauser, *Coord. Chem. Rev.* **1991**, *111*, 275–290.
[26] A. Hauser in *Spin Crossover in Transition Metal Compounds III* (Eds.: P. Gütlich, H. A. Godwin), Springer, Berlin, **2004**, pp. 155–198.
[27] J.-F. Létard, G. Chastanet, O. Nguyen, S. Marcén, M. Marchivie, P. Guionneau, D. Chasseau, P. Gütlich, *Monatsh. Chem.* **2003**, *134*, 165–183.
[28] G. S. Matouzenko, J.-F. Létard, S. Lecocq, A. Boussezsou, L. Capes, L. Salmon, M. Perrin, O. Kahn, A. Collet, *Eur. J. Inorg. Chem.* **2001**, 2935–2945.

Received: August 3, 2005
Published online: December 9, 2005

